Date of submission of revised manuscript: 1 April 2015

Ability of three different soil constitutive models to predict a tunnel's response to basement excavation

C. W. W. Ng[1, 2], H. S. Sun[3], G. H. Lei[4], J. W. Shi[5], David Mašín[6]

[1] Chair Professor, Department of Civil and Environmental Engineering, The Hong Kong University of Science and Technology, Clear Water Bay, Kowloon, Hong Kong SAR. E-mail: cecwwng@ust.hk

[2] Former "Chang Jiang Scholars Program" Chair Professor, Key Laboratory of Geomechanics and Embankment Engineering of the Ministry of Education, Geotechnical Research Institute, Hohai University, 1 Xikang Road, Nanjing 210098, China

[3] PhD student, Key Laboratory of Geomechanics and Embankment Engineering of the Ministry of Education, Geotechnical Research Institute, Hohai University, 1 Xikang Road, Nanjing 210098, China. E-mail: sunhuadasheng@126.com

[4] Professor, Key Laboratory of Geomechanics and Embankment Engineering of the Ministry of Education, Geotechnical Research Institute, Hohai University, 1 Xikang Road, Nanjing 210098, China. E-mail: leiguohui@hhu.edu.cn

[5] PhD student, Department of Civil and Environmental Engineering, The Hong Kong University of Science and Technology, Clear Water Bay, Kowloon, Hong Kong SAR. E-mail: shijiangwei@ust.hk

[6]Associate Professor, Department of Engineering Geology, Institute of Hydrogeology, Engineering Geology and Applied Geophysics, Faculty of Science, Charles University in Prague, Prague, Czech Republic. E-mail: masin@natur.cuni.cz

Corresponding author: Mr Sun Huasheng
Geotechnical Research Institute, Hohai University
1 Xikang Road, Nanjing 210098, China.
Telephone: 86 13770526749
E-mail: sunhuadasheng@126.com

ABSTRACT

Many constitutive models are available nowadays to predict soil-structure interaction problems. It is sometimes not very easier for engineers to select a suitable soil model to carry out their design analyses in terms of complexity versus accuracy. This paper describes the application of three constitutive models to back-analyse a well-instrumented centrifuge model test, in which the effect of basement excavation on an existing tunnel was simulated. These three models include a linear elastic-perfectly plastic model with the Mohr-Coulomb failure criterion (called MC model), a nonlinear elastic Duncan-Chang model (DC) and a hypoplastic model (HP), the last of which can capture the state-, strain- and path-dependent soil stiffness even at small strains and path- and state-dependent soil strength. By comparing with measured data from the centrifuge model test, it is found that the HP model yielded the best predictions of tunnel heave among the three models. Not only the gradient but also the magnitude of tunnel heave is predicted well by this HP model. This can be explained by the fact that the HP model can capture the state-, strain- and path-dependent soil stiffness even at small strains and path- and state-dependent soil strength but not the MC and DC models. However, all three models underestimated the change in tunnel diameter and the maximum tensile bending strain in the transverse direction.

Key words: constitutive model; numerical modelling; small-strain stiffness; tunnel heave

Introduction

A great challenge in the design and construction of basement excavation in urban areas is the protection of adjacent underground structures such as existing tunnels. Stress relief due to excavation causes additional stress and deformation which may affect the safety and serviceability of the existing tunnel. Prediction of tunnel deformation and stress distribution induced by excavation is becoming one of the major tasks for geotechnical engineers. The use of the finite element method to analyse the interaction between basement excavation and an existing tunnel is gaining popularity (Lo and Ramsay 1991; Doležalová 2001; Sharma et al. 2001; Zheng and Wei 2008; Huang et al. 2013; Ng et al. 2013). However, any prediction is only as good as the model with which it is made. Consequently, it is crucial to have a realistic soil behaviour model with which to estimate the magnitude and distribution of strain and deformation around an existing tunnel.

Among other things, a soil model must be able to capture soil non-linear stress-strain behaviour even at small strains. The degradation of shear modulus with strain has been widely recognised and well understood (Seed and Idriss 1970; Iwasaki et al. 1978; Simpson 1992; Mair 1993; Jovicic and Coop 1997; Oztoprak and Bolton 2013). The stiffness of a soil cannot be assumed to be constant when the strain around a geotechnical structure rises to a certain value. The degradation of stiffness with small strain should be considered when analysing deformation problems. Otherwise, the soil-structure interaction computation may be misleading (Jardine et al. 1986; Ng and Lings 1995; Addenbrooke et al. 1997; Hejazi et al. 2008; Mašín 2009; Svoboda et al. 2010).

Many constitutive models have been used to investigate the interaction between basement excavation and an existing tunnel, such as the linear elastic-perfectly plastic models with Mohr-Coulomb failure criteria (e.g., Lo and Ramsay 1991; Doležalová 2001; Sharma et al. 2001), the modified Cam-clay models (e.g., Zheng and Wei 2008), the hardening soil models (e.g., Huang et al. 2013), and the hypoplastic models (e.g., Ng et al. 2013). The most frequently used one for analysing the soil-structure interaction problem is a linear elastic-perfectly plastic Mohr-Coulomb model. But the question is whether a simple soil model is sufficient for serviceability design or whether a complex nonlinear soil model really provides a better solution. The ability of each model to predict the response of an existing tunnel to stress relief during basement excavation should be evaluated quantitatively. Moreover, there should be guidelines for selecting an appropriate model.

This paper evaluates the ability of different models to predict a tunnel's response to a nearby excavation quantitatively by back-analysing Ng et al.'s (2013) centrifuge model test. Numerical simulations are conducted using a Mohr-Coulomb model, a nonlinear Duncan-Chang model, and a hypoplastic model. Results computed from these three models are compared with those measured in the centrifuge model test. The comparisons of the model predictions can be regarded as the verifications of different design analyses carried out by various practicing engineers. As practising engineers are most interested in the maximum tunnel heave, the gradient of tunnel heave, the change in tunnel diameter and the tunnel bending strain, these are the aspects examined in this study.

Description of the simulated centrifuge test

A three-dimensional centrifuge model test (shown in Fig. 1) of a tunnel that runs parallel to and beneath a basement was carried out to investigate the effect of a new basement excavation on an existing tunnel in dry sand. The centrifuge test was conducted using the centrifuge on the campus of the Hong Kong University of Science & Technology (HKUST) (Ng et al. 2001, Ng et al. 2002). The aluminium model container had internal dimensions of 1245 mm (length) by 990 mm (width) by 850 mm (depth). The test was performed at a centrifuge acceleration of 60 g. Figs. 1(a) and (b) show elevation views of the centrifuge test. A square excavation (on plan) was carried out with length of 300 mm (equivalent to 18 m in prototype). The depth of the excavation was 150 mm (equivalent to 9 m in prototype). The penetration depth of the model wall was 75 mm (equivalent to 4.5 m in prototype). The soil sample consisted of dry Toyoura sand and was prepared by the pluvial deposition method. Both the model tunnel and the model diaphragm wall were made of an aluminium alloy with Young's modulus (E_a) of 70 GPa. The length, diameter and thickness of the model tunnel were respectively 1200 mm, 100 mm and 3 mm (approximately equivalent to 72 m, 6 m and 0.18 m in prototype). The model wall consisted of four aluminium plates with depth (H) and thickness (w) of 255 mm and 12.7 mm, respectively. The sample density was 1542 kg/m^3, corresponding to a relative density of 68%. As shown in Fig. 1, linear variable differential transformers (LVDTs) were used to measure soil heave at the formation level, ground surface settlement, and tunnel vertical displacement. Bending strain was measured with strain gauges (SGs). Four potentiometers were installed on the tunnel lining to measure changes in tunnel diameter. Basement excavation was modelled by draining the heavy fluid ($ZnCl_2$) from the flexible rubber bag to a reservoir. Three excavation stages were modelled according to measurement from the pore pressure transducers placed in the heavy fluid. Details of centrifuge model packages and results can be found in Ng et al. (2013). All results are presented in prototype scale here unless stated otherwise.

Finite element analysis

Finite element mesh and boundary conditions

The finite element program ABAQUS (ABAQUS, Inc. 2006) was used to simulate the effect of basement excavation on the existing tunnel. Fig. 2 shows the three-dimensional finite element mesh adopted in this analysis. The mesh dimensions were 1200 mm (length) by 990 mm (width) by 750 mm (depth). An eight-node brick element was used to simulate the sand, the diaphragm wall, and a four-node shell element was used to simulate the tunnel.

Pin supports were applied on all vertical sides and the base of the mesh to restrain movement in any direction (x, y or z direction).

In all the numerical analysis, interface elements were used at soil-tunnel and soil-basement wall interfaces, unless stated otherwise. Each interface element used is described by zero-thickness slip element assigned with the Coulomb friction law. The friction coefficient (μ) and limiting relative displacement (γ_{lim}) at which slippage occurs are controlled by two input parameters for each slip element. The interface friction coefficient, μ, is derived from $\mu=\tan\delta$, where δ is the interface friction angle, which is taken as 20° (i.e., 2/3 of the critical friction angle of soil). The limiting displacement of 5 mm is assumed to achieve full mobilisation of the interface friction.

Constitutive model and model parameters

Three constitutive models were used to simulate the behaviour of Toyoura sand used in the centrifuge model test: a linear elastic-perfectly plastic Mohr-Coulomb model, a nonlinear Duncan-Chang model and a hypoplastic model.

The Mohr-Coulomb model

The Mohr-Coulomb (MC) model is often used to simulate soil behaviour in general and serves as a first-order model. It has five parameters to describe the linear elastic-perfectly plastic behavior of soil. Two of these parameters come from Hooke's law (Young's modulus E and Poisson's ratio v). Another two parameters are used to define the failure criteria (the friction angle φ and cohesion c). The final parameter is called the dilatancy angle ψ, which is used to model a realistic irreversible change in volume due to shearing.

The initial vertical stress in soil elements at the tunnel centreline is about 231 kPa. Based on Bolton's (1986) investigation, the dilatancy angle ψ is calculated to be approximately 6° using equation (1):

(1) $$\psi = 3\left[D_r\left(10-\ln p'\right)-1\right]$$

where D_r is the relative density of sand and p' is the effective stress.

According to the calibration of Herle and Gudehus (1999), the critical friction angle φ_{cr} of Toyoura sand is 30°. Bolton (1986) formulated the following equation describing the relationship between critical friction φ_{cr} and the peak friction angle φ_p:

(2) $$\varphi_p = \varphi_{cr} + 0.8\psi$$

Thus, the peak friction angle is 35°.

The cohesion was taken to be 2 kPa in this numerical analysis for a static equilibrium in the MC model (ABAQUS, Inc. 2006). Young's modulus can be determined from the stiffness degradation curve of Toyoura sand (Iwasaki et al. 1978) as shown in Fig. 3.

According to Mair (1993), the strain of a soil surrounding a tunnel typically varies from 0.03% to 1%. The corresponding maximum and minimum values of secant shear modulus (G_{sec}) are 83 MPa and 7 MPa, respectively, as shown in Fig. 3. Thus, the average secant shear modulus (G_{sec}) is 45 MPa. Considering the elastic domain parameters of the MC model are user-defined, the Young's modulus of 117 MPa is obtained with Poisson's ratio 0.3 adopted (Zhang et al. 2010). It is noted that the soil strains reported by Mair (1993) were for the surrounding soil response to tunnelling construction. For the soil response to an excavation, the induced shear strain may be smaller. Considering that it is more common for engineers to use an averaged soil stiffness when the MC model is adopted, however, the soil stiffness corresponding to 0.1% axial strain was thus selected.

The Duncan-Chang model

The Duncan-Chang (DC) model is an incremental nonlinear stress-dependant model which is also known as the hyperbolic model (Duncan and Chang 1970). The DC model adopted in this paper specifies 11 parameters (K, n, R_f, c, φ_0, G, D, F, K_{ur}, p_a and $\Delta\varphi$). Readers should refer to Duncan and Chang (1970) and Kulhawy and Duncan (1972) for their physical meaning. All 11 parameters can be obtained from standard triaxial tests in which the intermediate principal stress is made identical to the minor principal stress. As for Toyoura sand used in the DC model, the friction angle φ_0 was taken to be 35° as in the MC model. The cohesion c was set to 2 kPa for the static equilibrium. The atmospheric pressure p_a used in the formulation to eliminate the unit system selection effect was 101 kPa. The parameters K and n can be determined from the stress-strain ((σ_1 – σ_3)-ε_a) curve based on triaxial tests conducted by Maeda and Miura (1999). K_{ur} is the unloading-reloading modulus number and is often 2–3 times larger than the initial tangent modulus number K for many geomaterials (Duncan and Chang 1970). The dimensionless parameters G, D, and F can be obtained from the relationship between the maximum principal strain and minor principal strain (ε_a-ε_r) based on the triaxial tests performed by Maeda and Miura (1999). According to Duncan and Chang (1970), the value of R_f ranges from 0.75 to 1 for a number of different soils and is essentially independent of confining pressure. For simplicity, the value of R_f was taken to be 0.8 in this paper. All parameters used in the DC model are summarised in Table 1.

The hypoplastic model

It is well known that nonlinearity has a significant influence on predicted ground movements (Ng et al. 1995; Powrie et al. 1998; Atkinson 2000; Clayton 2011). The nonlinearity of soil can be captured by a hypoplastic (HP) constitutive model. Various HP models have been developed in the 1990s (Kolymbas 1991; Gudehus 1996; Von Wolffersdorff 1996; Wu et al. 1996) as well as recently (Mašín 2012, 2013, 2014). The model proposed by Von Wolffersdorff (1996) was adopted to describe the behaviour of Toyoura sand. This model was incorporated into the software package ABAQUS using open-source implementation which can be freely downloaded from the web (Gudehus et al. 2008). The model specifies eight material parameters (φ'_c, h_s, n, e_{d0}, e_{c0}, e_{i0}, α and β). Niemunis and Herle (1997) improved the model for predictions of small-strain stiffness and the recent stress history, leading to five additional parameters (m_T, m_R, R, β_r and χ). See Table 2 and the literature mentioned above for their physical meaning.

Six parameters of Toyoura sand (φ'_c, h_s, n, e_{d0}, e_{c0} and e_{i0}) were obtained from Herle and Gudehus (1999), while the triaxial test results reported by Maeda and Miura (1999) were used to calibrate the parameters of α and β. Five parameters (m_T, m_R, R, β_r and κ) of the intergranular strain can be calibrated from the stiffness degradation curve of Toyoura sand (Iwasaki et al. 1978) as shown in Fig. 3. The void ratio of soil was considered as a state variable in the HP model. All parameters adopted in the HP model are summarised in Table 2.

Comparison between model prediction and drained triaxial test

Parameters of each model were obtained through the above analyses. For comparisons, the same drained triaxial test was simulated using all three models. Fig. 4a compares the model-predicted stress-strain curve and the measured one. The experimental data are taken from Maeda and Miura (1999). Fig. 4b shows the comparisons of model-predicted stiffness-strain curves using three different constitutive models based on experimental data reported by Maeda and Miura (1999). It is clear that the major difference between the three models is the capability of predicting strain-dependent soil stiffness at strains less than 0.1%. The curves simulated by the DC and HP models in Fig. 4a and 4b are comparable, although an exact match could not be obtained because of rather different model frameworks. Fig. 4c shows the comparisons of model-predicted volumetric-axial strain curves using three different constitutive models based on experimental data reported by Maeda and Miura (1999). Compressive strains are taken as positive quantities. It is found that HP model can predict the relationship between volumetric strain and axial strain reasonably while it is not the case of MC and DC models.

Based on a large amount of laboratory tests and calibration, parameters of the Toyoura sand of each model were obtained for simulating the centrifuge model test. It should be stressed out that the HP model, unlike the other models involved, has the parameters independent of the initial state (see Hájek et al., 2009). Then, it is not important to ensure the experiments have been performed at the same relative density as the centrifuge test; the model adjusts the response automatically. This is not the case of the other two models. The tunnel lining and diaphragm wall were modelled as linear elastic materials. The unit weight of the aluminium alloy used for the model tunnel lining and diaphragm wall was 30 kN/m^3. Young's modulus and Poisson's ratio of the aluminium alloy were 70 GPa and 0.2, respectively.

Numerical modelling procedures

The numerical modelling procedure is the same as that in the centrifuge test. Whereas excavation in centrifuge model test was simulated by draining away the heavy fluid ($ZnCl_2$), in numerical modelling excavation it was achieved by decreasing the horizontal and vertical pressures via the following steps:

1. Establish the initial stress conditions using K_0=0.5. Apply the same amounts of vertical and horizontal pressure as in the centrifuge test to the formation level and the diaphragm wall, respectively.
2. Incrementally increase the gravitational acceleration of the whole model from 1 g to 60 g in four steps, i.e., from 1 g, to 15 g, to 30 g, to 45 g, and finally to 60 g. Simultaneously, apply pressure to the formation level and the wall.
3. Decrease the amounts of vertical and horizontal pressure gradually in each excavation stage to simulate excavation until a depth of 9 m is reached.

Comparisons between measured and computed results

Soil heave at the formation level of the basement

Fig. 5 compares the measured and computed normalised soil heave at the formation level of the basement. H_{ec} is the excavation depth and H_e is the final excavation depth. The

MC model overestimated soil heave at the formation level by 75%, 41%, and 54% after the first, second, and final excavation stages, respectively, whereas the DC model underestimated the soil heave by 28%, 42% and 37%. The results computed with the HP model agree with the measured results for the first two stages of excavation. For the third excavation stage, however, the HP model predicted a slightly larger (i.e. 37% larger) soil heave than the measured. This is because soil stiffness in the HP model decreases as strain increases. It was found that the HP model can predict soil heave better than the other two constitutive models. The simple MC model may still be used for preliminary estimation of soil heave subject to the inaccuracy revealed above.

Tunnel heave along its longitudinal direction

Tunnel displacement governs the curvature and bending moment of a tunnel, and so it is important for practising engineers to be able to predict it. Fig. 6a compares the measured tunnel heave along its longitudinal direction with that computed using the three different models. It can be seen from Fig. 6a that after the first stage of excavation, the MC model overestimated tunnel heave by 58%, whereas the DC and HP models underestimated the same parameter by 30% and 2%, respectively. However, the both MC and DC models overestimated tunnel heave even at a distance of 2.3(L/2) (where L is the basement length) away from the basement centre. As the excavation proceeded to the second stage, the MC model and HP model overestimated the maximum tunnel heave by 42% and 4%, respectively, while the DC model underestimated it by 35%. Both the MC and DC models also severely overestimated tunnel heave even at places far away from the diaphragm wall. This means that in practice, neither model should be used to predict tunnel heave. After basement excavation, the MC model overestimated the tunnel heave beneath the basement centre (by 46%) and also that behind the diaphragm wall. Meanwhile, the DC model underestimated the tunnel heave beneath the basement centre by 33% but overestimated it at some distance away from the basement centre. The HP model overestimated the maximum tunnel heave by 19% and was able to predict the heave behind the diaphragm wall consistently. Thus it can be concluded that the HP model does a better job of predicting tunnel heave than either the MC or the DC model not only in terms of magnitude but also in terms of distribution. The large differences in predictive ability between the three models indicate the importance of taking into account the effect of small-strain stiffness.

Fig. 6b shows the gradient of tunnel heave against the distance from the basement centre after excavation. The absolute gradients of tunnel heave increased within the basement but decreased outside the basement with distance away from the basement centre. The absolute gradient of tunnel heave reached a maximum at the diaphragm wall. Thus special attention should be paid to this region in practice. It is noted that the MC model was able to predict the gradient of tunnel heave reasonably well. The reason may be that the soil stiffness used in the MC model overestimated the tunnel heave not only beneath the basement but also behind the diaphragm wall. The DC model, on the other hand, severely underestimated the tunnel heave gradient and thus should not be used to predict this particular parameter.

The analyses above show that the HP model has advantages over both the MC and DC models as it only overestimated the tunnel heave after excavation by 19% and it was able to predict the gradient of tunnel heave reasonably accurately. The HP model's superiority in this regard arises from its ability to capture the state-, strain- and path-dependent soil stiffness even at small strains and path- and state-dependent soil strength, which is something neither the MC model nor the DC model is capable of doing. According to the Land Transport Authority of Singapore (LTA 2000), the maximum tunnel movement should not exceed 15 mm (i.e., 0.17% H_e as shown in Fig. 6a). Both the computed and measured maximum tunnel heave in this study are within the proposed allowable limit. In practice, if results from the MC model were used (heave overestimated), the tunnel would need to be reinforced. On the other hand, if results from the DC model were used (heave underestimated), the basement excavation may lead to the collapse of the existing tunnel. Detailed comparisons between the measured and computed tunnel responses are summarised in Table 3.

Change in tunnel diameter

Fig. 7 compares the computed (with the three models) and measured change in tunnel diameter (D) with unloading ratio (H_{ec}/C), where C is the cover depth of tunnel. Positive and negative values denote elongation and compression of the tunnel, respectively. All three models predicted that the tunnel lining would be vertically elongated and horizontally compressed and the magnitude of elongation (ΔD_V) and compression (ΔD_H) would increase with excavation depth. The HP model gave slightly better predictions than did the MC and DC models, but all three underestimated the change in tunnel diameter by 34%, 66%, and 25% by the MC, DC and HP models, respectively. This may be due to the fact that the computed soil stiffness around the tunnel in the transverse direction is larger than that used in the centrifuge model test. According to the British Tunnelling Society (BTS 2000), the maximum distortion of a tunnel ((ΔD_V+ΔD_H)/D) should not exceed 2%. The maximum distortion of the existing tunnel (i.e., 0.16% D) induced by basement excavation in this study is within the proposed allowable limit. Although all of the computed and measured results are within the proposed allowable limit, all three models underestimated the change in tunnel diameter, which may lead to non-conservative or even problematic designs.

Bending strain in the transverse and longitudinal directions of the tunnel lining

Fig. 8a compares the measured and computed strains at the outer surface of the tunnel lining along its transverse direction after basement excavation. Positive and negative values denote tensile and compressive strains, respectively. The results computed with the three models are in reasonable agreement with the measured values. The computed strain profile is symmetrical. Tensile strain was found at the tunnel crown, shoulders, knees and invert, while compressive strain was recorded at the tunnel springlines. The MC, DC and HP models underestimated the maximum tensile bending strain in the transverse direction by 26%, 56% and 15%, respectively, for the same reason that they underestimated the change in tunnel diameter. The HP model gave the best predictions among the three models as shown in Fig. 8a. According to the American Concrete Institute (ACI 2001), the ultimate tensile strain of unreinforced concrete is 150 $\mu\varepsilon$. Both the computed and measured additional bending strains in the transverse direction are within the proposed allowable limit, assuming that there was no bending strain in the tunnel lining before excavation.

Fig. 8b compares the measured and computed strains at the tunnel crown along its longitudinal direction after basement excavation. Positive and negative values denote tensile and compressive strains, corresponding to hogging and sagging moments, respectively. The measured and computed results exhibit similar trends. Their profiles are symmetrical with respect to the basement centre. For the measured results, the maximum strain in the hogging regions is approximately four times larger than that in the sagging regions. For the computed results, the maximum strains in the hogging regions are approximately four, three and four times larger than those in the sagging regions for the MC, DC and HP models, respectively. The MC and HP models overestimated the maximum tensile strain in the hogging regions by 52% and 38%, respectively, while the DC model underestimated it by 24%, for the same reason that they failed to estimate the tunnel heave correctly. The MC model gave a maximum tensile bending strain of 105 $\mu\varepsilon$. Since the ultimate tensile strain of unreinforced concrete is 150 $\mu\varepsilon$ according to ACI224R (ACI 2001), cracks may appear in the tunnel if existing tensile strain is larger than 45 $\mu\varepsilon$.

The maximum bending strains of the tunnel were underestimated in the transverse direction but overestimated in the longitudinal direction by both the MC and HP models. The

DC model, however, underestimated the maximum tensile bending strain in both directions, because it does not capture path-dependent soil stiffness and the value it used after excavation is larger than that in the centrifuge model test. A summary of the comparisons is given in Table 3.

Analyses of predicted soil responses by the three models due to stress relief by the excavation

Stress and stiffness distributions of soil elements around the tunnel

In order to better understand the tunnel behaviour in the transverse and longitudinal directions, the stress and stiffness distributions of soil elements around the tunnel are shown in Figs. 9 and 10. Fig. 9a shows the computed changes in vertical stress at the tunnel crown in the longitudinal direction**.** Positive and negative values denote increases and decreases in stress acting on the tunnel lining, respectively. The three models predicted similar trends of vertical stress at the tunnel crown. Along the tunnel crown, the vertical stress beneath the basement is significantly reduced due to excavation. A stress relief that is almost uniform can be observed just beneath the basement. Stress is concentrated beneath the diaphragm wall due to the upward tunnel movement and downward soil-wall frictions. Thus, the vertical stress in the soil increased by more than 50 kPa. At a distance of 0.6 (L/2) (L is basement length) away behind the diaphragm wall, soil stress increased slightly (by less than 20 kPa) at the crown. After basement excavation, the maximum change in vertical stress at the tunnel crown exceeded the allowable limit (i.e., ±20 kPa) set by the Building Department of Hong Kong (BD 2009). Stress changes behind the diaphragm wall stayed within the allowable limit though.

The DC model predicted the largest stress change (in absolute value) in soil elements, then the MC model, while the HP model predicted the smallest change because of rather different model frameworks. However, the changes in vertical stress computed by all three models are not too large as shown in Fig. 9a, with the maximum change being less than 9%. This implies that the deformation of the tunnel lining is governed by the stiffness of soil around the tunnel.

Fig. 9b shows the relationships between the mobilised secant shear stiffness of soil at the tunnel crown and the normalised distance from the basement centreline. The mobilised secant shear stiffness after excavation (G_m) was normalised by the initial secant shear stiffness at maximum g-level (G_0) for each model. It can be seen from Fig. 9b that the secant shear stiffness does not change for the MC model while it significantly decreases for the DC model (by about 58% of G_0) and the HP model (by about 9% of G_0) especially for soil elements underneath the basement. The reason is that due to the removal of vertical stress at the tunnel crown (see Fig. 9a), shear strain increased in the soil, but unlike the DC and HP models, the MC model cannot capture the change in soil stiffness with strain. The larger the shear stiffness of soil, the larger the resistant force of soil which causes it to deform. Suppose that the initial secant shear stiffness G_0 is the same for each model. The HP model should predict the largest tunnel heave while the MC model should predict the smallest heave. However, as shown in Fig. 6, the MC model predicted the largest tunnel heave, the HP model predicted less and the DC model predicted the smallest heave. The reason is that the average stiffness after excavation is the smallest for the MC model, less for the HP model and the largest for the DC model. To prove this, the changes in stiffness in the soil elements around the tunnel were analysed using the three constitutive models as shown in Fig. 10. Stiffness computed with the MC model was always constant at any soil elements and any excavation stage. According to the DC model, stiffness reduced gradually with the increase in shear strain as the excavation proceeded, but did not change too much. According to the HP model, however, stiffness reduced substantially as the excavation went on. The HP model can capture precisely the changes in stiffness with strain, especially at small strains, as it is path-dependent and strain-dependent even at small strains. The DC model gave the largest average stiffness while the MC model yielded the smallest. It is important to understand why the DC model predicted the smallest tunnel heave while the MC model predicted the largest values of the parameter as shown in Fig. 6 as well as the largest bending strain as shown in Fig. 8.

Shear strain for soil elements around the tunnel

Fig. 11 shows the distribution of shear strain at soil elements located at the crown, shoulders, springlines and invert, around the tunnel in the transverse and longitudinal directions after excavation computed using the three different models. The transverse section shown in Fig. 11a is located at the basement centre (i.e. section S1 in Fig. 1a). The three models yielded similar distribution patterns and magnitudes of shear strain in soil elements around the tunnel lining. The maximum shear strain was recorded at the crown while the minimum shear strain was observed around the invert. The magnitude of shear strain in section S1 (see Fig. 1a) ranges from the minimum value of 0.02% around the invert to the maximum value of 0.14% at the crown. It seems that the stiffness adopted for any calculations based on a simple linear elastic-perfectly plastic model may be appropriate corresponding to the average strain level in soil elements around the tunnel due to basement excavation. In practice, design engineers can back-analyse relevant case records to obtain an average shear strain on an existing tunnel in a basement excavation. Thus, they can deduce the corresponding soil stiffness for their numerical analyses through laboratory soil tests. However, using simple models such as the MC model in this way may lead to more errors than using advanced models. Practitioners should use advanced models even if they have to estimate the parameters, rather than to use simple models with constant stiffness and elaborate calibration procedures based on back-analyses of simulated cases.

As the maximum shear strain was found at the crown while the minimum strain was found around the invert, Fig. 11b only shows the shear strain distributions at those places in the longitudinal direction after basement excavation. The magnitude of shear strain within the excavation zone around the tunnel and the retaining wall ranges from the minimum value of 0.02% to the maximum value of 0.34%. It can also be seen that within the excavation zone, similar to the section S1 at the basement centre (as shown in Fig. 11a), the maximum shear strain was observed at the crown and the minimum shear strain was recorded around the invert. The HP model predicted the largest shear strain while the DC model predicted the smallest at the crown. The MC and HP model predicted almost the same shear strain at the invert, while the DC model gave a slightly smaller value. The shear strain at the crown and the invert decreased dramatically and then gradually approached zero with the distance away from the diaphragm wall. In general, the HP model computed slightly larger shear strains than the other two models although the values were still of the same order of magnitude both within the excavation zone and behind the diaphragm wall. However, as a preliminary analysis, the MC model as a simple linear elastic-perfectly plastic model can be used to estimate the shear strain around an existing tunnel after basement excavation.

Significance of soil small-strain stiffness for practising engineers

It is possible to select an appropriate mean soil stiffness in a linear elastic-perfectly plastic analysis to predict tunnel displacement, tunnel diameter change and stress distribution in the soil around an existing tunnel due to basement excavation. However, soil stiffness cannot be taken as constant when strain around geotechnical structures increases to a certain value. For example, as shown in Fig. 6a, the maximum tunnel heave can be predicted using the MC model by selecting an appropriate stiffness value. However, a rather large tunnel heave is also computed at a distance away from the diaphragm wall which is unrealistic in practice. Neither the MC model nor the DC model can reliably predict the tunnel heave because neither model can capture the path-dependent stiffness at small strains. In practice, engineers are generally very concerned about tunnel heave around excavations in urban areas, since it governs the curvature and bending moment of the tunnel. Thus it is imperative that practising engineers consider soil small-strain stiffness in their designs.

Small-strain stiffness also has a significant influence on the interpretation of equivalent stiffness in centrifuge tests (as shown in Fig. 10). The simple linear elastic-perfectly plastic model (i.e., MC) and the non-linear elastic model (i.e., DC) are convenient tools for estimating soil stiffness. However, unless the fact that soil stiffness varies with small strains is taken into account, any computations of basement-soil-tunnel interaction and the interpretation of centrifuge test or field measurements can be misleading. The more advanced constitutive models that can capture small-strain stiffness such as the HP model involves more soil parameters and an understanding of numerical modelling and nonlinear soil behaviour. Whether linear analysis or nonlinear analysis should be conducted depends on how precise the results are required to be and what resources are available.

Conclusions

This paper has evaluated the predictivity of three constitutive models by back-analysing a centrifuge model test that simulated the response of an existing tunnel during basement excavation. These models used include a linear elastic-perfectly plastic model with the Mohr-Coulomb failure criterion (called MC model), a nonlinear Duncan-Chang model and a hypoplastic model. The comparisons of the model predictions can be regarded as the verifications of different design analyses carried out by various practicing engineers. Based on the comparisons between measured and computed results, the following conclusions may be drawn:

(a) Due to stress relief by the basement excavation, the HP model predicted soil heaves at all three stages of the excavation better than those by the other two models consistently.

This is because the HP was able to capture the variations of soil stiffness with strains and stress paths.

(b) The DC model mobilised the largest soil stiffness at the final stage of excavation, while the MC model mobilised the least. For the given amount of stress relief by the excavation, both MC and HP models overestimated the maximum tunnel heave by 46% and 19%, respectively, while the DC model underestimated it by 33%. The HP model better predicted not only the magnitude but also the gradient of measured tunnel heave.

(c) The MC, DC and HP models underestimated the measured change in tunnel diameter by 34%, 66%, and 25%, respectively. Consistently with the predictions of change in tunnel diameter, the maximum tensile bending strain in the transverse direction was underestimated by all three models. The MC, DC and HP models underestimated the measured maximum strain by 26%, 56% and 15%, respectively. All these predictions are not on the conservative side for design.

(d) Both the MC and HP model overestimated the maximum bending strain in the longitudinal direction (i.e., by 52% and 38% respectively). However, the DC model underestimated the measured value by 24%, consistent with its underestimation of tunnel heave.

Acknowledgements

This study was sponsored by the Program for Chang Jiang Scholars and Innovative Research Team in University (grant number IRT1125), the 111 Project (grant number B13024), the Fundamental Research Funds for the Central Universities of China (grant number 2010B28114 and 2014B04914), the Chang Jiang Scholars Program of the Ministry of Education of China, the research grant GRF 617511 awarded by RGC, and research grants M-HKUST603/13 and 20130094140001 provided by the Specialized Research Fund for the Doctoral Program of Higher Education.

References

ABAQUS, Inc., 2006. ABAQUS User's and Theory Manuals. Version 6.6, Providence Rhode Island, USA: ABAQUS, Inc.

Addenbrooke, T.I., Potts, D.M., Puzrin, A.M., 1997. The influence of pre-failure soil stiffness on the numerical analysis of tunnel construction. Géotechnique, 47 (3): 693-712.

ACI. 2001. Control of cracking in concrete structures (ACI 224R-01). American Concrete Institute (ACI), Mich., USA.

Atkinson, J.H., 2000. 40th Rankine Lecture. Non-linear soil stiffness in routine design. Géotechnique, 50 (5): 487-508.

BD. 2009. Practice note for authorized persons APP-24. Technical notes for guidance in assessing the effects of civil engineering construction/building development on railway structures and operations. Building Department of the Government of HKSAR (BD).

Bolton, M.D., 1986. The strength and dilatancy of sands. Géotechnique, 36 (1): 65-78.

BTS (2000). Specification for tunnelling. British Tunnelling Society (BTS). Thomas Telford, London.

Clayton, C.R.I., 2011. 50th Rankine Lecture. Stiffness at small strain: research and practice. Géotechnique, 61 (1): 5-37.

Doležalová, M., 2001. Tunnel complex unloaded by a deep excavation. Computers and Geotechnics, 28 (6): 469-493.

Duncan, J.M., Chang, C.Y., 1970. Nonlinear analysis of stress and strain in soils. Journal of the Soil Mechanics and Foundations Division, ASCE, 96: 1629-1653.

Gudehus, G., 1996. A comprehensive constitutive equation for granular materials. Soils and Foundations, 36 (1): 1-12.

Gudehus, G., Amorosi, A., Gens, A., Herle, I., Kolymbas, D., Mašín, D., Muir Wood, D., Niemunis, A., Nova, R., Pastor, M., Tamagnini, C., Viggiani, G., 2008. The soilmodels.info project. International Journal for Numerical and Analytical Methods in Geomechanics, 32 (12): 1571-1572.

Hájek, V., Mašín, D. and Boháč, J., 2009. Capability of constitutive models to simulate soils with different OCR using a single set of parameters. Computers and Geotechnics, 36 (4): 655-664.

Hejazi, Y., Dias, D., Kastner, R., 2008. Impact of constitutive models on the numerical analysis of underground constructions. Acta Geotechnica, 3 (4): 251-258.

Herle, I., Gudehus, G., 1999. Determination of parameters of a hypoplastic constitutive model from properties of grain assemblies. Mechanics of Cohesive-frictional Materials, 4: 461-486.

Huang, X., Schweiger, H.F., and Huang. H.W., 2013. Influence of deep excavations on nearby existing tunnels. International Journal of Geomechanics, ASCE, 13 (2): 170-180.

Iwasaki, T., Tatsuoka, F., Takagi, Y., 1978. Shear moduli of sands under cyclic torsional shear loading. Soils and Foundations, 18 (1): 39-50.

Jovicic, V., Coop, M.R., 1997. Stiffness of coarse-grained soils at small strains. Géotechnique, 47 (3): 545-561.

Jardine, R.J., Potts, D.M., Fourie, A.B., Burland, J.B., 1986. Studies of the influence of non-linear stress strain characteristics in soil structure interaction. Géotechnique, 36 (3): 377-396.

Kolymbas, D. 1991. An outline of hypoplasticity. Archive of Applied Mechanics, 61: 143-151.

Kulhawy, F.H., Duncan, J.M., 1972. Stresses and movements in Oroville Dam. Journal of the Soil Mechanics and Foundations Division, ASCE, 98 (SM7): 653-655.

LTA. 2000. Code of practice for railway protection. Development & Building Control Department, Land Transport Authority (LTA), Singapore.

Lo, K.Y., Ramsay, J.A., 1991. The effect of construction on existing subway tunnels-a case study from Toronto. Tunnels and Deep Space, 6 (3): 287-297.

Maeda, K., Miura, K., 1999. Confining stress dependency of mechanical properties of sands. Soils and Foundations, 39 (1): 53-67.

Mair, R.J., 1993. Developments in geotechnical engineering research: application to tunnels and deep excavations. Proceedings of the Institution of Civil Engineers: Civil Engineering, 97 (1): 27-41.

Mašín, D., 2009. 3D modelling of a NATM tunnel in high K_0 clay using two different constitutive models. Journal of Geotechnical and Geoenvironmental Engineering, ASCE, 135 (9): 1326-1335.

Mašín, D., 2012. Hypoplastic Cam-clay model. Géotechnique, 62 (6): 549-553.

Mašín, D., 2013. Clay hypoplasticity with explicitly defined asymptotic states. Acta Geotechnica, 8 (5): 481-496.

Mašín, D., 2014. Clay hypoplasticity model including stiffness anisotropy. Géotechnique, 64 (3): 232-238.

Ng, C.W.W., Lings, M.L., 1995. Effect of modeling soil nonlinearity and wall installation on back-analysis of deep excavation in stiff clay. Journal of Geotechnical Engineering, ASCE, 21 (10): 687-695.

Ng, C.W.W., Lings, M.L., Simpson, B., Nash, D.F.T., 1995. An approximate analysis of the three-dimensional effects of diaphragm wall installation. Géotechnique, 45 (3): 497-507.

Ng, C.W.W., Shi, J.W., Hong, Y., 2013. Three-dimensional centrifuge modelling of basement excavation effects on an existing tunnel in dry sand. Canadian Geotechnical Journal, 50 (8): 874-888.

Ng, C.W.W., Van Laak, P.A., Tang, W.H., Li, X.S., Zhang, L.M., 2001. The Hong Kong geotechnical centrifuge. Proc. 3rd Int. Conf. Soft Soil Engineering, 225-230.

Ng, C.W.W., Van Laak, P.A., Zhang, L.M., Tang, W.H., Zong, G.H., Wang, Z.L., Xu, G.M., Liu, S.H., 2002. Development of a four-axis robotic manipulator for centrifuge modeling at HKUST. Proc. Int. Conf. Physical Modelling in Geotechnics, St. John's Newfoundland, Canada, 71-76.

Niemunis, A., Herle, I., 1997. Hypoplastic model for cohensionless soils with elastic strain range. Mechanics of Cohesive-frictional Materials, 2: 279-299.

Oztoprak, S., Bolton, M.D., 2013. Stiffness of sands through a laboratory test database. Géotechnique, 63 (1): 54-70.

Powrie, W., Pantelidou, H., Stallebrass, S.E., 1998. Soil stiffness in stress paths relevant to diaphragm walls in clay. Géotechnique, 48 (4): 483-494.

Seed, H.B., Idriss, I.M., 1970. Soil moduli and damping factors for dynamic response analyses, Report EERC 70-10. Berkeley, CA, USA: University of California.

Simpson, B., 1992. Retaining structures: displacement and design. Géotechnique, 42 (4): 541-576.

Sharma, J.S., Hefny, A.M., Zhao, J., Chan, C.W., 2001. Effect of large excavation on displacement of adjacent MRT tunnels. Tunnelling and Underground Space Technology, 16 (2): 93-98.

Svoboda, T., Mašín, D. and Boháč, J. 2010. Class A predictions of a NATM tunnel in stiff clay. Computers and Geotechnics, 37 (6): 817-825.

Von Wolffersdorff, P.A., 1996. A hypoplastic relationship for granular material with a predefined limit state surface. Mechanics of Cohesive-frictional Materials, 1: 251-271.

Wu, W., Bauer, E., Kolymbas, D., 1996. Hypoplastic constitutive model with critical state for granular materials. Mechanics of Materials, 23 (1): 45-69.

Zhang, F., Jin, Y., Ye, B., 2010. A try to give a unified description of Toyoura sand. Soils and Foundations, 50 (5): 679-693.

Zheng, G., Wei, S.W., 2008. Numerical analysis of influence of overlying pit excavation on existing tunnels. Journal of Central South University of Technology, 15 (s2): 69-75.

LIST OF CAPTIONS

Table 1. Soil parameters used in the Duncan-Chang model

The modulus number (a dimensionless material parameter), K	1584
Modulus exponent (a dimensionless material parameter), n	0.5
Failure ratio, R_f	0.8
Cohesion, c	2 kPa
Friction angle at the unit atmospheric pressure of confining pressure σ_3, φ_0	35°
Material parameter, G	0.3
Material parameter, D	27.9
Material parameter, F	0.034
Unloading-reloading modulus number (a dimensionless material parameter), K_{ur}	3168
The atmospheric pressure that is used in the formulation to eliminate unit system selection effect, p_a	101 kPa
The reduction in φ for a tenfold increase in σ_3, $\Delta\varphi$	0

Table 2. Soil parameters used in the hypoplastic model

Critical state friction angle(1), φ_c	30°
Granulates hardness(1), h_s	2.6 GPa
Exponent n(1), n	0.27
Minimum void ratio at zero pressure(1), e_{d0}	0.61
Critical void ratio at zero pressure(1), e_{c0}	0.98
Maximum void ratio at zero pressure(1), e_{i0}	1.10
Exponent α(2), α	0.14
Exponent β(2) , β	3.0
Parameter controlling the initial shear modulus upon a 180° strain path reversal and in the initial loading(2), m_R	5.5
Parameter controlling the initial shear modulus upon a 90° strain path reversal(2), m_T	2.75
Size of elastic range(2), R	3×10^{-5}
Parameter controlling rate of degradation of stiffness with strain(2), β_r	0.08
Parameter controlling rate of degradation of stiffness with strain(2), χ	1.0
Coefficient of at-rest earth pressure, K_0	0.5
Dry density, ρ_d	1542 kg/m^3
Void ratio, e	0.72

Note: (1) Herle and Gudehus, 1999
(2) Obtained by fitting test results from Iwasaki et al. (1978) and Maeda and Miura (1999)

Table 3. Comparison of computed and measured values

Parameter	Mohr-Coulomb	Duncan-Chang	Hypoplastic
Max. tunnel heave	+46%	−33%	+19%
Gradient of tunnel heave	Good	poor	Very good
Max. change in tunnel diameter	−34%	−66%	−25%
Max. bending strain in transverse direction	−26%	−56%	−15%
Max. bending strain in longitudinal direction	+52%	−24%	+38%

Note: The -ve sign indicates an underestimate and the +ve indicates an overestimate

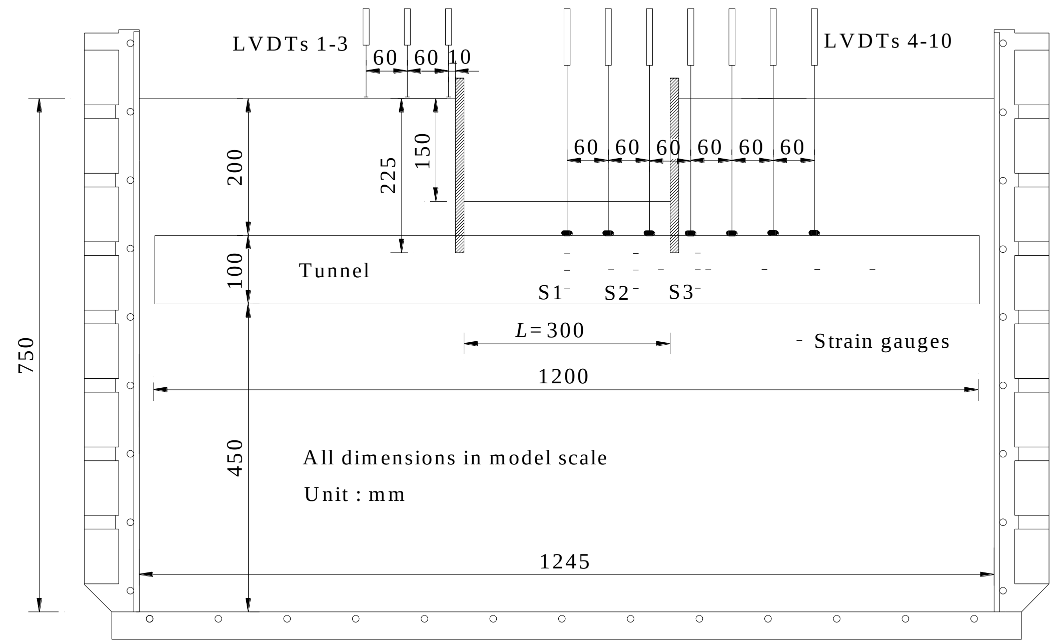

(a)

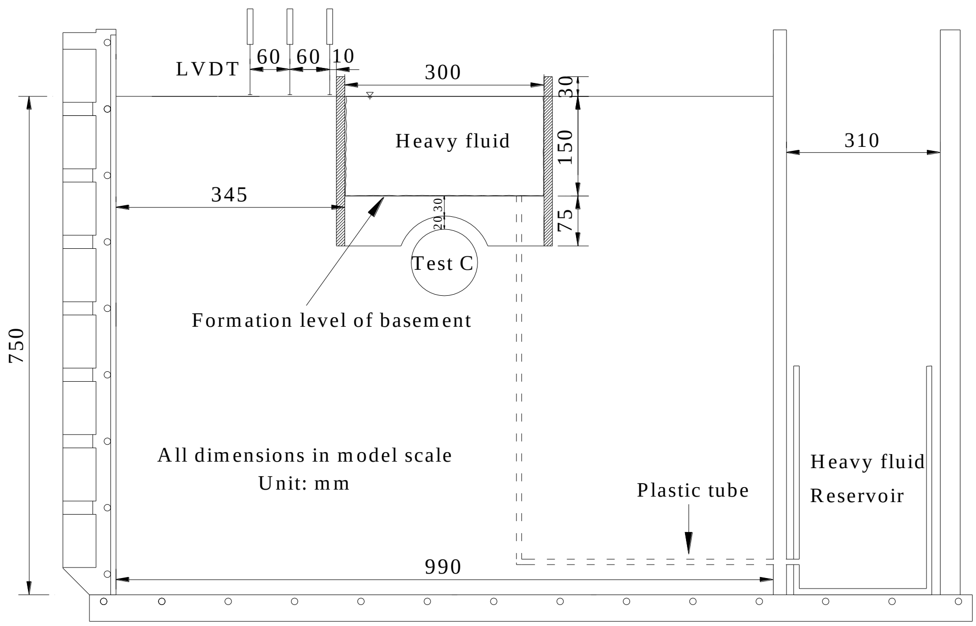

(b)

Fig. 1. Elevation views of the centrifuge model: (a) longitudinal direction; (b) transverse direction (all dimensions in model scale, unit: mm).

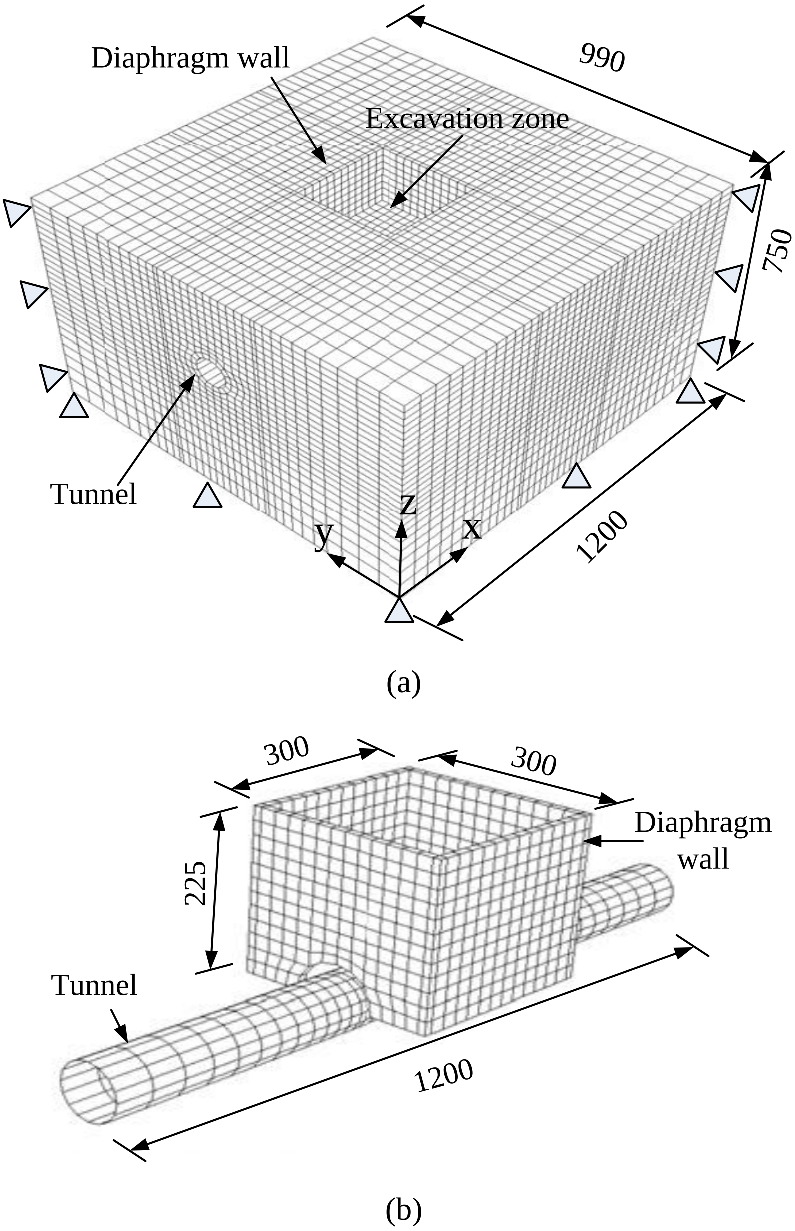

Fig. 2. (a) Three-dimensional finite element model adopted in this study (all dimensions in model scale, unit: mm); (b) intersection of the tunnel and diaphragm wall.

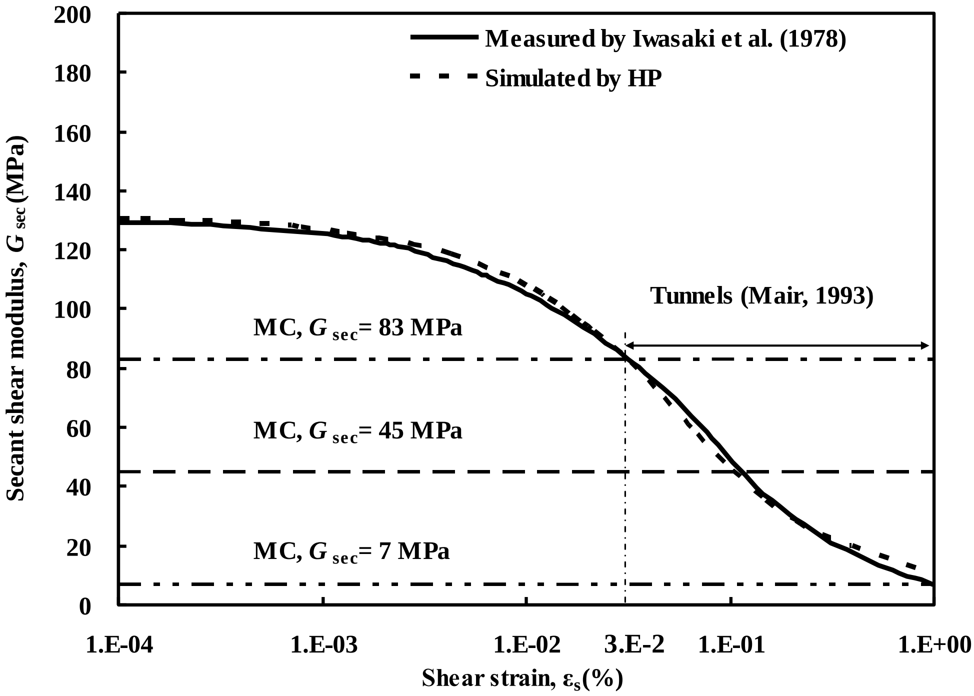

Fig. 3. Calibrations of secant shear modulus versus shear strain of Toyoura Sand.

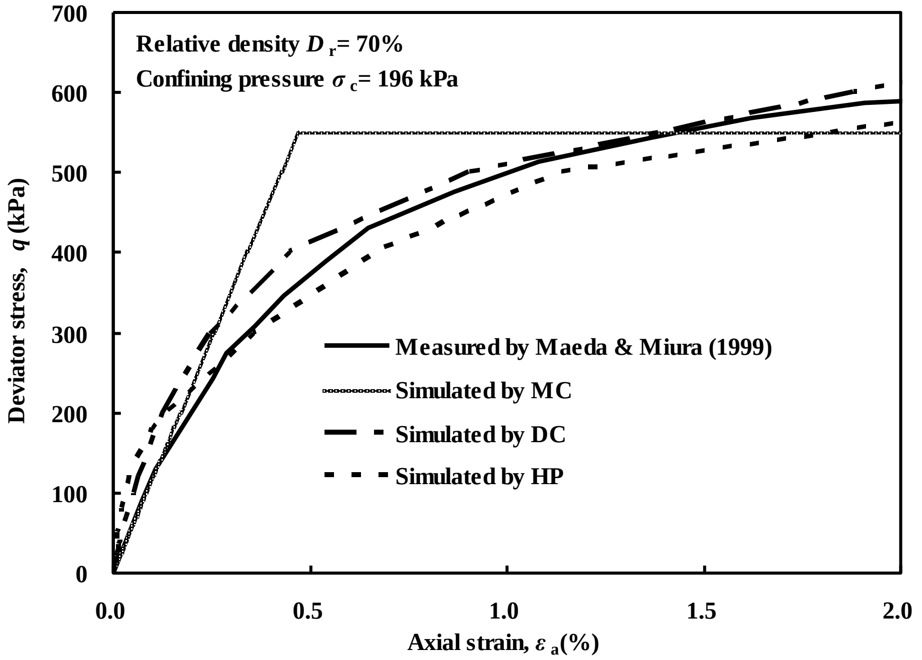
Relative density D_r= 70%
Confining pressure σ_c= 196 kPa
Measured by Maeda & Miura (1999)
Simulated by MC
Simulated by DC
Simulated by HP
Deviator stress, q (kPa)
Axial strain, ε_a(%)
0
100
200
300
400
500
600
700
0.0
0.5
1.0
1.5
2.0

(a)

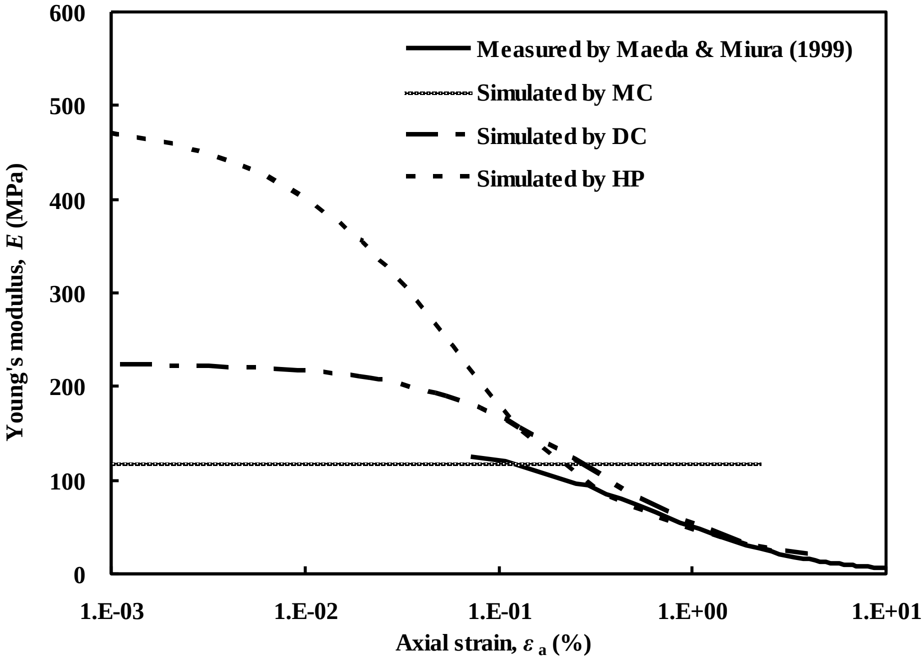
Measured by Maeda & Miura (1999)
Simulated by MC
Simulated by DC
Simulated by HP
Young's modulus, E (MPa)
Axial strain, ε_a (%)
0
100
200
300
400
500
600
1.E-03
1.E-02
1.E-01
1.E+00
1.E+01

(b)

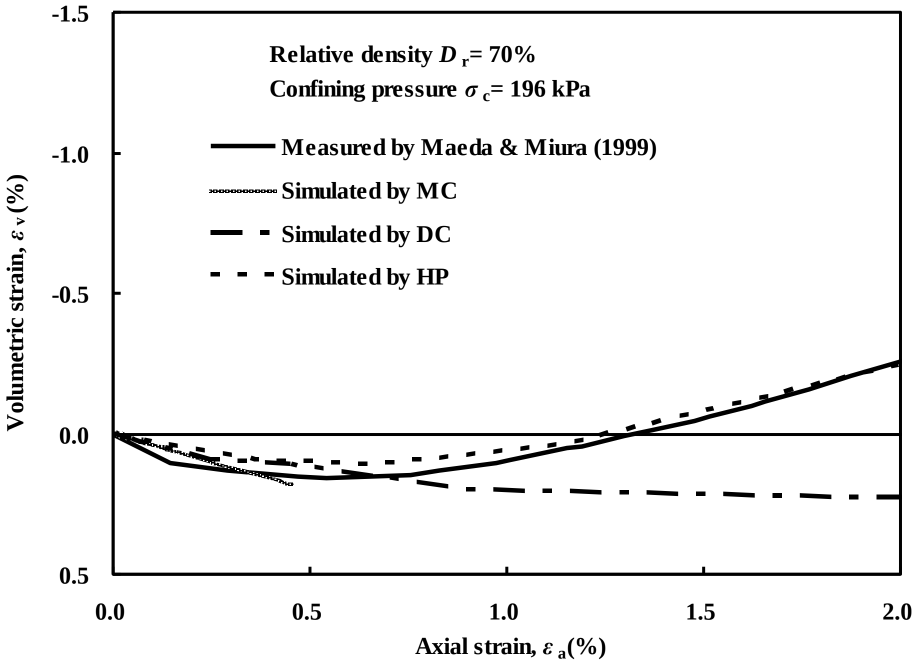

(c)

Fig. 4. A comparison of the measured and computed (a) stress-strain curves; (b) stiffness-strain curves; (c) volumetric-axial strain curves (experimental data are taken from Maeda and Miura, 1999).

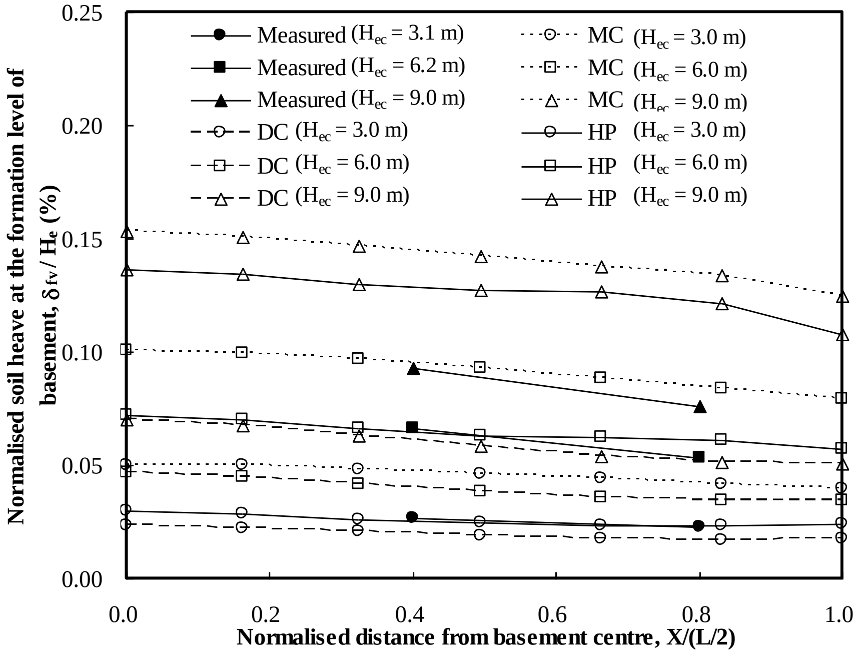

Fig. 5. A comparison of the measured and computed basement heave.

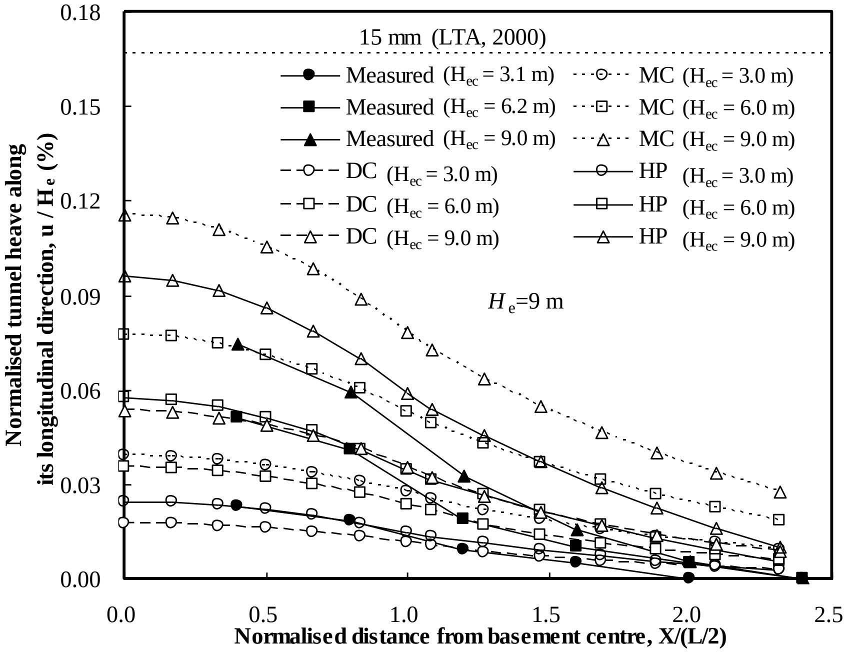

(a)

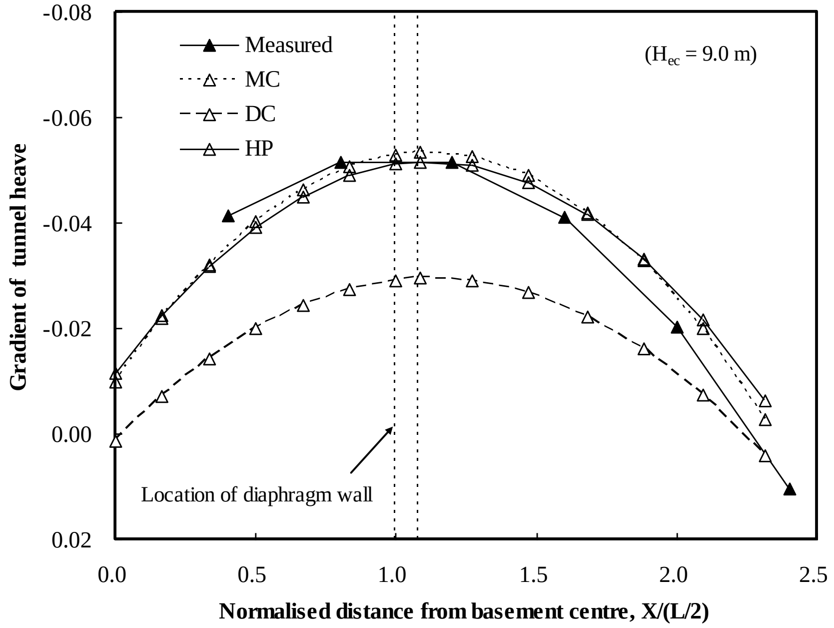

(b)

Fig. 6. A comparison of the measured and computed (a) tunnel heave and (b) gradient of tunnel heave.

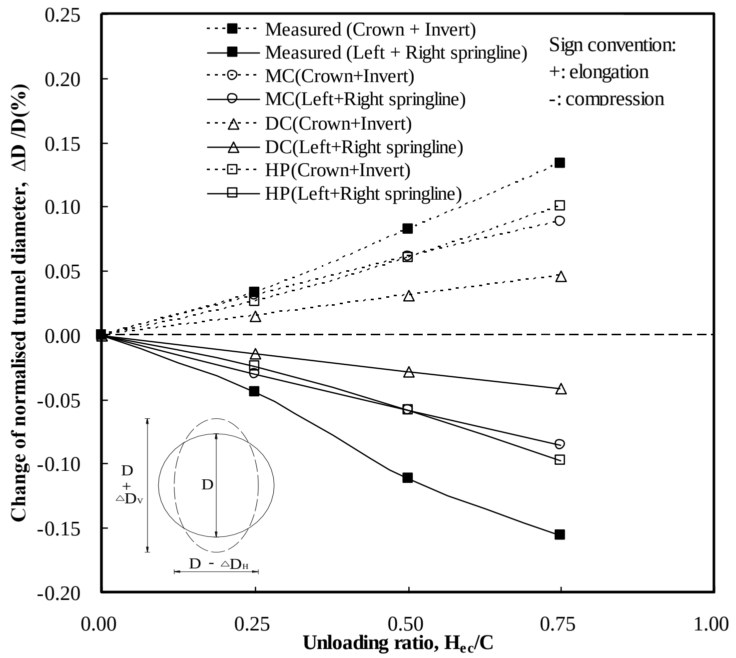

Fig. 7. A comparison of the measured and computed change in tunnel diameter.

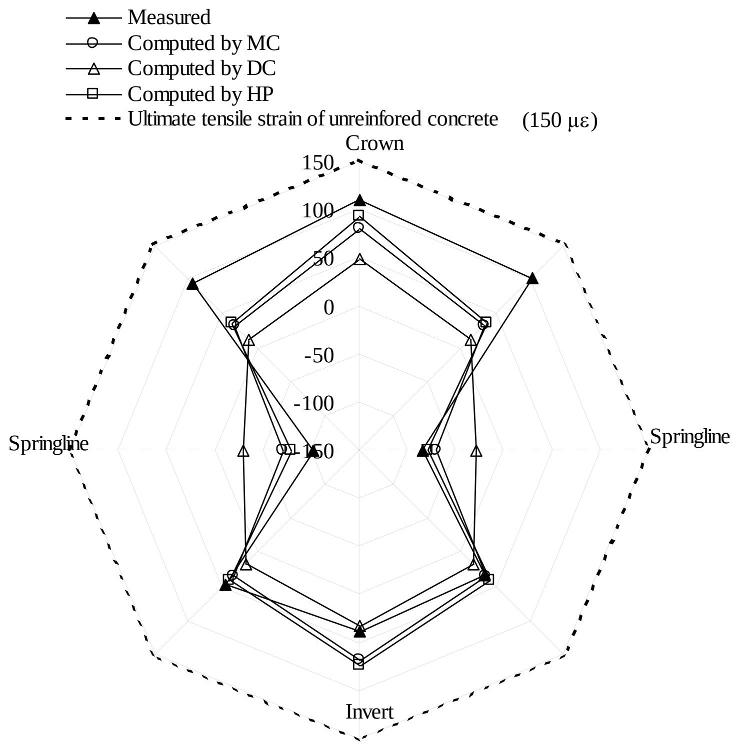

(a)

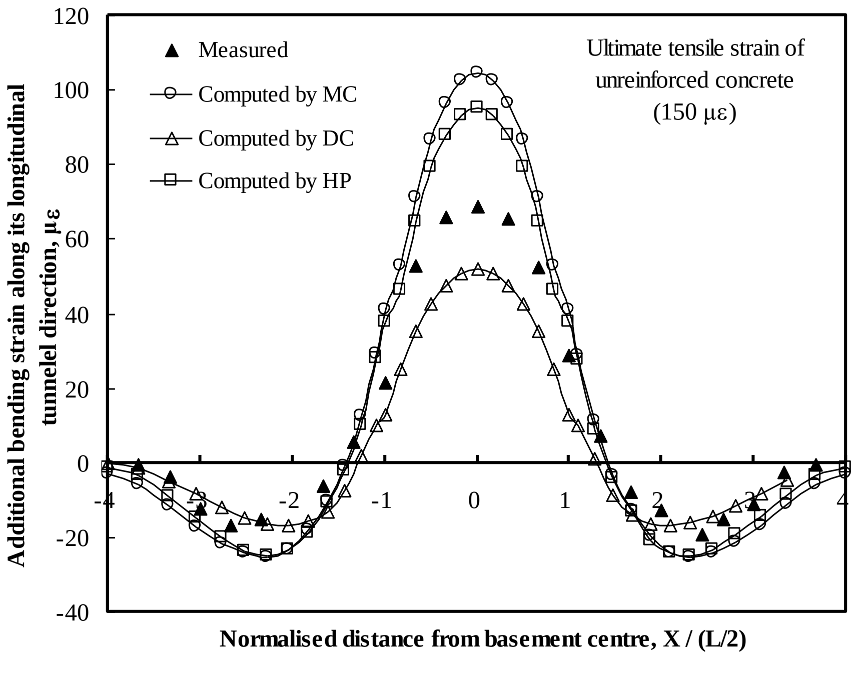

(b)

Fig. 8. A comparison of the measured and computed additional bending strains along (a) the transverse section S1 and (b) the longitudinal direction of the tunnel.

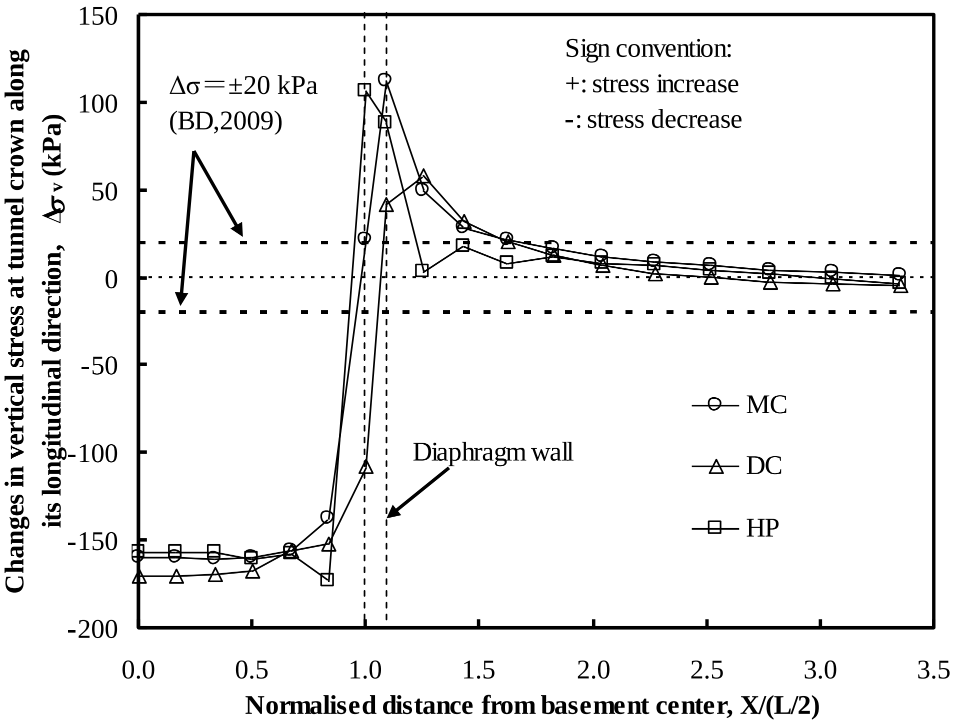

(a)

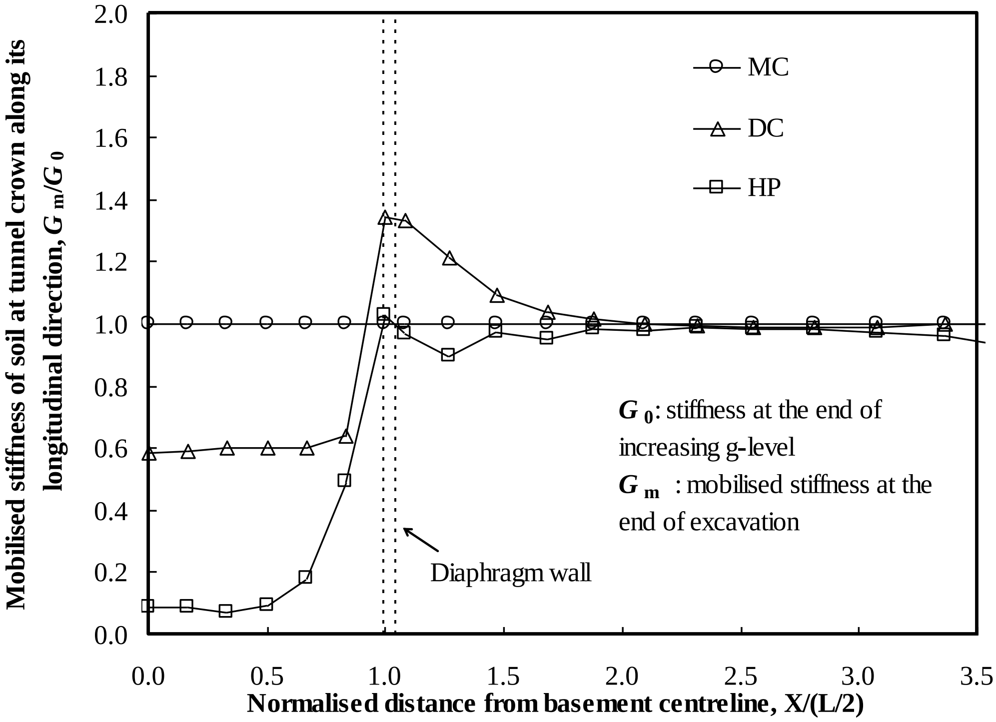

(b)

Fig. 9. A comparison of the soil responses around the tunnel along its longitudinal direction computed with the three models: (a) changes in vertical stress at the crown; (b) mobilised stiffness of soil at the crown.

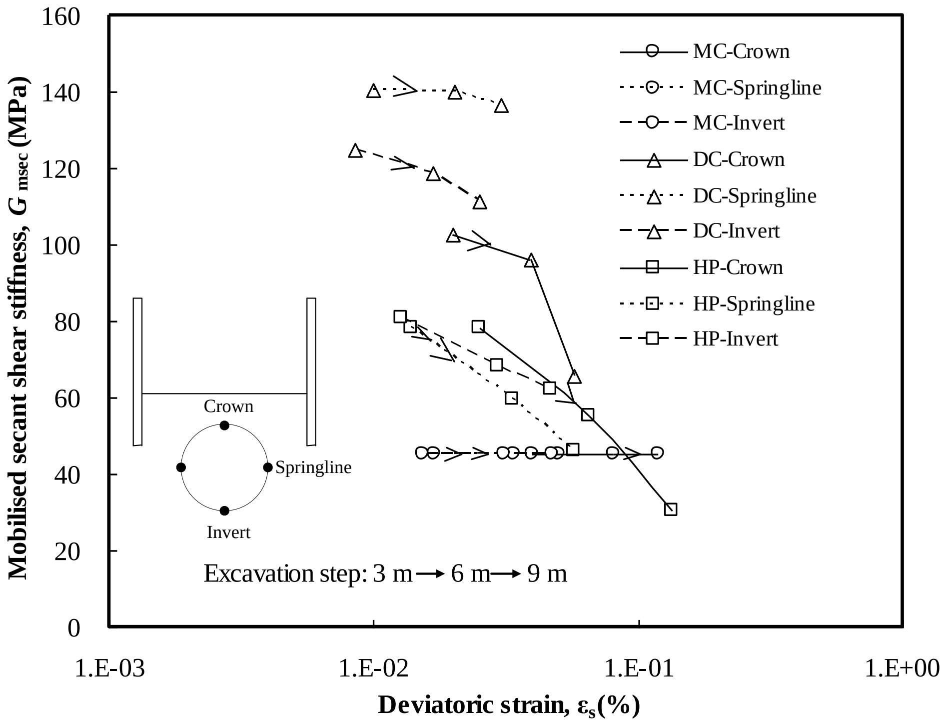

Fig. 10. Stiffness-strain curves for soil elements around the tunnel.

(a) Transverse direction

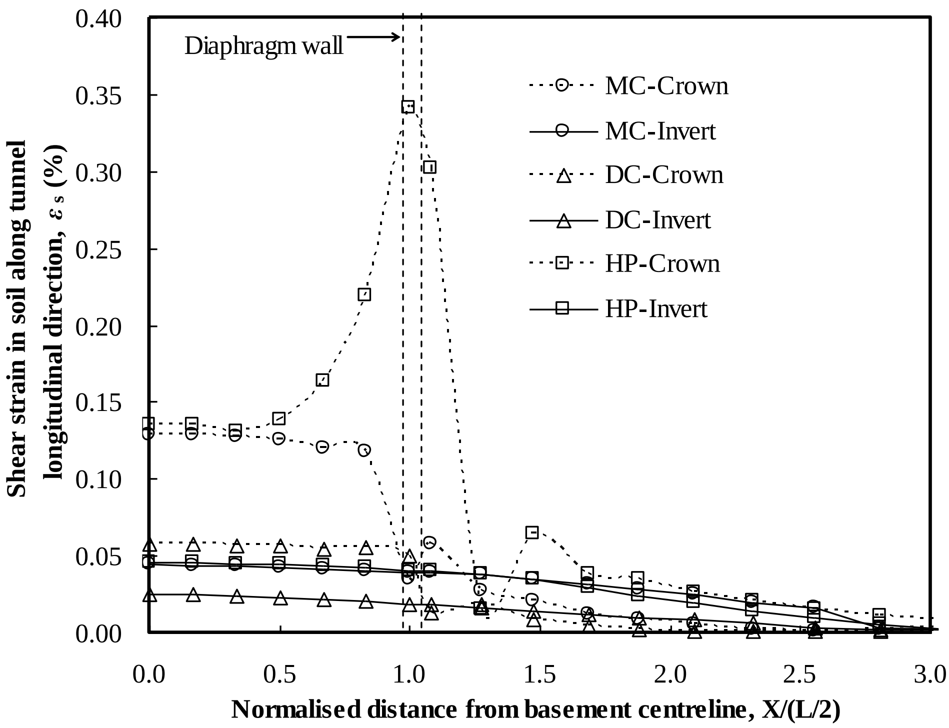

(b) Longitudinal direction

Fig. 11. Comparison of shear strain in (a) the transverse direction and (b) the longitudinal direction for soil elements around the tunnel.